Adiabatic compression of elongated fieldreversed configurations

R. L. Spencer, M. Tuszewski, and R. K. Linford

Citation: Physics of Fluids (1958-1988) **26**, 1564 (1983); doi: 10.1063/1.864334
View online: http://dx.doi.org/10.1063/1.864334
View Table of Contents: http://scitation.aip.org/content/aip/journal/pof1/26/6?ver=pdfcov
Published by the AIP Publishing

Adiabatic compression of elongated field-reversed configurations

R. L. Spencer, M. Tuszewski, and R. K. Linford
Los Alamos National Laboratory, University of California, Los Alamos, New Mexico 87545

(Received 6 December 1982; accepted 24 February 1983)

The adiabatic compression of an elongated field-reversed configuration (FRC) is computed by using a one-dimensional approximation. The one-dimensional results are checked against a two-dimensional equilibrium code. For ratios of FRC separatrix length to separatrix radius greater than about ten, the one-dimensional results are accurate within 10%. To this accuracy, the adiabatic compression of FRC's can be described by simple analytical formulas.

I. INTRODUCTION

One of the interesting aspects of field-reversed-configuration (FRC) research is the possibility of translating these objects after formation into a different area where they would be compressed.[1] Indeed, the results of such an experiment were recently reported by Es'kov and his coworkers.[2] The computational modeling of this process on dynamic time scales is very expensive; it would help if there were a simpler way to at least approximately predict what would happen in such experiments. The simplest model of plasma dynamics is the adiabatic model. In this model the plasma is assumed to be in magnetohydrodynamic (MHD) equilibrium at each instant of time. The equilibria are connected by the requirement that they all have the same entropy per unit flux, i.e., the equilibria form a sequence generated by adiabatic changes. A way of computing such a sequence of equilibria was developed by Grad[3] and applied to FRC's by Byrne, Grossmann, and Hameiri.[4,5] Even these much simpler computations require complicated computer codes. It would be helpful if approximately the same results could be achieved either with a much simpler code or by analytical techniques. Methods for accomplishing this simplification for elongated FRC's are presented in this paper. In Sec. II a one-dimensional equilibrium code is described and its results are checked against a two-dimensional equilibrium code; in Sec. III an even simpler analytic calculation is presented.

II. ONE-DIMENSIONAL ADIABATIC MODEL

Elongated FRC equilibria can very nearly be described as two regions with straight field lines connected by a short transition region with curved field lines.[6] This property makes it possible to extract two-dimensional information from one-dimensional calculations. The average-beta condition is obtained by this procedure.[7] This property of elongated FRC's will be exploited here to obtain an approximate model for adiabatically changing FRC equilibria.

Consider an elongated FRC in a conducting cylinder of radius r_w as shown in Fig. 1. It has magnetic flux $2\pi\psi_0$ outside of the separatrix and magnetic flux $2\pi\psi_t$ inside the separatrix. It has pressure profile $p(\psi)$, where ψ is the poloidal flux function, and separatrix length l. We restrict our discussion to the case where the pressure vanishes on and outside the separatrix; the pressure is also assumed to rise monotonically from the separatrix to its maximum value p_m at the equilibrium vortex point. Imagine now that an initial equilibrium is adiabatically changed by slowly varying either r_w or ψ_0. Note that reversibility of adiabatic changes makes it possible to consider these two different kinds of changes separately. Under adiabatic changes ψ_t is conserved and the magnetofluid is tied to the field lines. Hence, the condition that entropy per unit flux be conserved reduces to the condition

$$\mu_f(\psi) = \mu_i(\psi), \tag{1}$$

where the subscripts "i" and "f" refer to equilibria before and after the adiabatic change, respectively, and where

$$\mu(\psi) = p(\psi)\left(2\pi \oint \frac{dl}{B}\right)^{\gamma}. \tag{2}$$

The line integral is taken along the closed field lines; μ, like p, is zero outside the separatrix. We now make the one-dimensional approximation by writing

$$\oint \frac{dl}{B} \simeq \frac{2l}{B} = \frac{2l}{\{2[p_m - p(\psi)]\}^{1/2}}, \tag{3}$$

where radial pressure balance for the straight field line region inside the separatrix has been used to obtain the final form. This approximation eliminates the transition region where the field lines are curved and represents the magnetofluid by a cylinder of straight field lines of length l. This approximate form for the line integral is clearly wrong at the vortex point: in the two-dimensional equilibrium the elliptical shape of the flux surfaces gives a finite value for the line integral at the vortex point, while Eq. (3) has a singularity there. The approximation is also wrong at the separatrix where it gives a finite value; the spindle point where $B = 0$ makes the line integral be infinite there. For elongated equilibria, however, the approximation is not as bad as might be expected. For such equilibria the surfaces are so elongated at

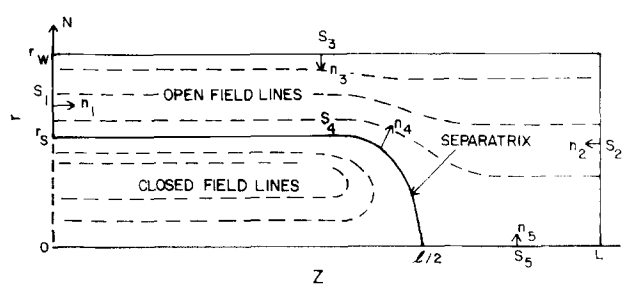

FIG. 1. A field-reversed configuration inside a cylindrical flux conserver.

 0031-9171/83/061564-05$01.90

the vortex point that a finite but very large value for the line integral is obtained; furthermore, the singularity at the separatrix is only logarithmic, and hence is very weak. Figure 2 compares the correct line integral with the approximation for an elongated equilibrium.

If the pressure profile is written in the form $p(\psi) = p_m \beta(\phi)$, where $\phi = \psi/\psi_t$, then Eq. (1) becomes a condition relating initial and final β profiles:

$$\frac{\beta_f(\phi)}{[1-\beta_f(\phi)]^{\gamma/2}} = A \frac{\beta_i(\phi)}{[1-\beta_i(\phi)]^{\gamma/2}}, \tag{4}$$

where

$$A = (l_i/l_f)^{\gamma}(p_{mi}/p_{mf})^{1-\gamma/2}. \tag{5}$$

Note that for all values of A, if $0 \leqslant \beta_i \leqslant 1$, then $0 \leqslant \beta_f \leqslant 1$. Because of the average-beta condition, a β profile uniquely determines a FRC equilibrium given r_w and ψ_0 (Ref. 6). A method for computing FRC profiles at the equilibrium midplane where the field lines are nearly straight is described in the Appendix of Ref. 6. It is now possible to outline a procedure for computing the final equilibrium from the initial one.

(1) Choose an initial equilibrium by specifying β_i, r_{wi}, and ψ_{0i}. Given these quantities, p_{mi} and ψ_{ti} are determined.

(2) Choose r_{wf} or ψ_{0f} and vary A until Eq. (4) gives the β profile that makes an equilibrium with $\psi_{ti} = \psi_{tf}$. The results of this one-dimensional equilibrium calculation are midplane profiles of pressure and magnetic field in the final state.

(3) Solve Eq. (5) for l_f.

This procedure is relatively easy to carry out, especially if the one-dimensional equilibrium solver is like the one described in Ref. 6. It uses numerical integration and zero finding to determine important parameters, so the determination of A can easily be added to the algorithm. The only extra difficulty is that Eq. (4) must be solved. Because of its complicated form for arbitrary γ, it is best solved numerically. A simple and rapidly converging iteration scheme for solving Eq. (4) is given by

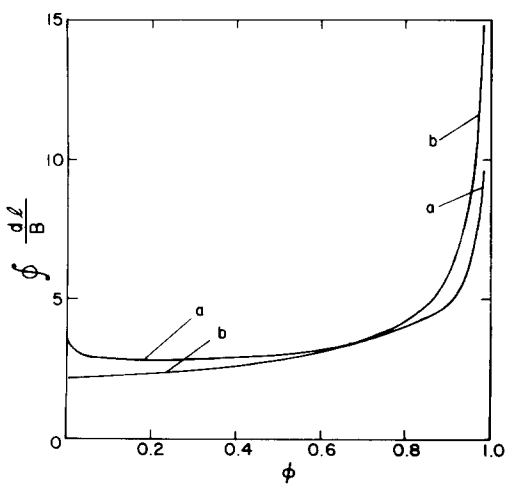

FIG. 2. The function $\oint(dl/B)$ (a) and its one-dimensional approximation (b) in arbitrary units. These functions are obtained from an equilibrium with $x_s = 0.9$ and $l/r_s = 15.6$.

$$\beta_f^{n+1} = \frac{1}{1 + C(1-\beta_f^n)^{1-\gamma/2}}, \tag{6}$$

where $C = (1-\beta_i)^{\gamma/2}/(A\beta_i)$.

In the case of flux compression, i.e., changing ψ_0, the full procedure is required. However, the procedure is quite simple in the case of wall compression for which ψ_0 and ψ_t are held fixed, for then their ratio is fixed and is given by

$$\frac{\psi t}{\psi_0} = \frac{x_s^2}{2(1-x_s^2)} \int_0^1 (1-\beta)^{1/2} du, \tag{7}$$

where x_s is the ratio of r_s, the midplane separatrix radius, to the wall radius and where $u = 2r^2/r_s^2 - 1$. The β profile is a function of u through its dependence on $\phi(r)$ after the equilibrium has been determined. Suppose now that β_f is gotten from β_i according to Eq. (4). It is easy to see that if $A > 1$, then $\beta_f > \beta_i$ and that if $A < 1$, then $\beta_f < \beta_i$. The average-beta condition can be written in the form

$$\langle \beta \rangle = \int_0^1 \beta \, du = 1 - \frac{x_s^2}{2}. \tag{8}$$

From Eq. (8) we see that if $A > 1$, then $x_{sf} < x_{si}$ and that if $A < 1$, then $x_{sf} > x_{si}$. Now consider Eq. (7); if $A > 1$, then both x_s and $(1-\beta)^{1/2}$ decrease, causing the flux ratio to decrease; conversely if $A < 1$, the flux ratio increases. Hence, for wall compression in the one-dimensional approximation, $A = 1$: the pressure profile does not change shape. Using Eq. (5) and the relation $p_m \propto \psi_0^2/r_w^4$, the dependence of l on the wall radius can be found to be

$$l_f/l_i = (r_{wf}/r_{wi})^{(4-2\gamma)/\gamma}. \tag{9}$$

This expression agrees with previous work on wall compression in this approximation.[8] For the case of $\gamma = \frac{5}{3}$ the scaling of l with r_w is $l \propto r_w^{2/5}$.

To test the accuracy of the one-dimensional approximation, we use Hewett's two-dimensional FRC equilibrium code[6] as follows. We choose an initial $p(\psi)$ profile and compute a final $p(\psi)$ profile from the one-dimensional approximation. These profiles are then used in the two-dimensional code and the lengths of the initial and final equilibria are adjusted so that the ratio l_f/l_i predicted by the one-dimensional approximation is obtained. The functions $\mu_i(\psi)$ and $\mu_f(\psi)$ are then computed by properly calculating the line integrals on the two-dimensional mesh. If the one-dimensional approximation were exact, the two functions μ so computed would coincide. They do not agree precisely, but they are close for highly elongated equilibria, as shown in Figs. 3 and 4. The initial profile used in these calculations is $\beta(\phi) = (\phi + \sigma\phi^2)/(1+\sigma)$. The parameter σ can be adjusted to obtain any desired value of x_s. In the examples that follow, the initial equilibrium had $x_s = 0.9$. Figure 3 shows three μ profiles obtained from the two-dimensional code using three pressure profiles that are adiabatically connected through wall compression according to the one-dimensional approximation.

For elongations (l/r_s) greater than about 12, the one-dimensional approximation is accurate within about 10%. The approximation is quite poor when the elongation is less than about eight. Figure 4 shows μ profiles similarly ob-

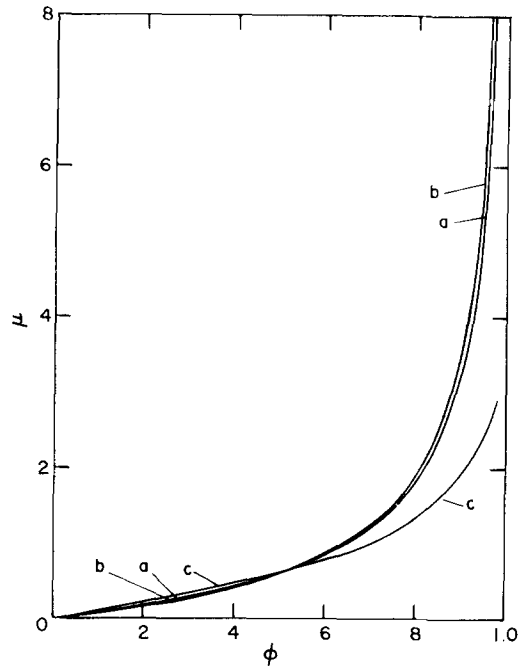

FIG. 3. The $\mu(\phi)$ profiles (arbitrary units) for three equilibria adiabatically connected according to the one-dimensional approximation to wall compression. The initial equilibrium (a) has $x_s = 0.9$ and $l/r_s = 14.6$. The wall-compressed equilibrium (b) has $x_s = 0.9$ and $l/r_s = 22.5$. The wall-decompressed equilibrium (c) has $x_s = 0.9$ and $l/r_s = 6.9$. Equilibrium (c) is not elongated enough for the one-dimensional approximation to be accurate.

tained for the case of flux compression. In this case 10% accuracy is obtained for elongations greater than about eight. These requirements on the elongation are satisfied by most experiments.

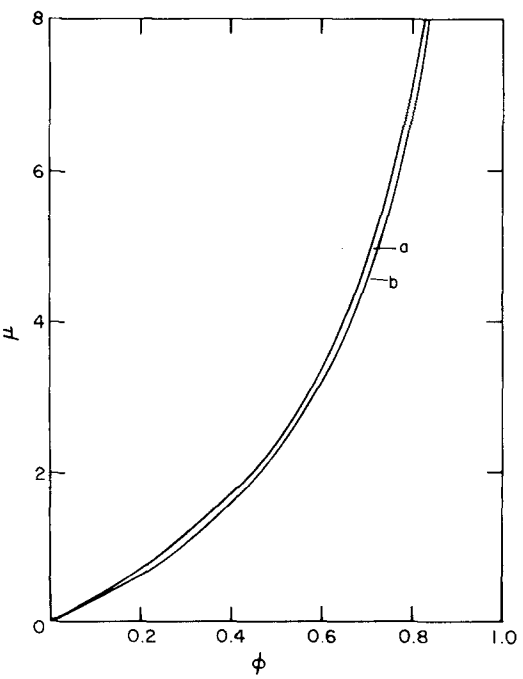

FIG. 4. The $\mu(\phi)$ profiles (arbitrary units) for two equilibria adiabatically connected according to the one-dimensional approximation to flux compression. The initial equilibrium (a) has $x_s = 0.9$ and $l/r_s = 15.6$. The flux-compressed equilibrium (b) has $x_s = 0.6$ and $l/r_s = 8.1$.

III. ANALYTICAL MODEL

We consider an elongated FRC equilibrium inside a straight cylindrical flux conserver as shown in Fig. 1. As in Sec. II, the separatrix is modeled as a cylinder of length l and radius r_s and we consider the adiabatic compression of the FRC by changes in r_w and ψ_0 (e.g., wall and flux compressions, respectively). The energy balance within the separatrix can be written as

$$dE = dW, \tag{10}$$

where $E = \int [p/(\gamma - 1) + B^2/2\mu_0]dV$ is the total energy within the separatrix volume V and where dW is the work done on the separatrix by the external magnetic field pressure. With the above assumptions and using Eq. (8), we obtain $E = p_m V[1 - (2 - \gamma)x_s^2/2]/(\gamma - 1)$ and, therefore,

$$dE = E\left(\frac{2\,dr_w}{r_w} + 2\frac{dx_s}{x_s} + \frac{dl}{l} + \frac{dp_m}{p_m} - \frac{x_s\,dx_s(2-\gamma)}{1-(2-\gamma)x_s^2/2}\right). \tag{11}$$

The dW term is evaluated in the Appendix as

$$dW = -p_m V\left(2\frac{dr_w}{r_w} + 2\frac{dx_s}{x_s} + (1 - x_s^2)\frac{dl}{l}\right). \tag{12}$$

The trapped magnetic flux inside the separatrix can be written as

$$2\pi\psi_t = \pi r_w^2 B_w x_s^3/2f, \tag{13}$$

with $f = x_s/\int_0^1 (1-\beta)^{1/2}du$. We assume that f is only a function of x_s, or equivalently, that the change in pressure profile $\beta(u)$ only comes from varying x_s. Then, using Eq. (13), the relations $\psi_t = \text{const}$ and $p_m \propto B_w^2$ can be used to obtain

$$\frac{dp_m}{p_m} = -2(3-\epsilon)\frac{dx_s}{x_s} - 4\frac{dr_w}{r_w}, \tag{14}$$

where $\epsilon = (x_s/f)(df/dx_s)$. Equations (8), (10)–(12), and (14) can be combined to obtain

$$\frac{dl}{l} = \frac{(4-2\gamma)}{\gamma}\frac{dr_w}{r_w} + \frac{2(3-\gamma-\epsilon)}{\gamma}\frac{dx_s}{x_s} - \frac{(1+\epsilon-\gamma\epsilon)}{\gamma}\frac{d\langle\beta\rangle}{\langle\beta\rangle}. \tag{15}$$

For wall compression, x_s is constant and integrating Eq. (15) gives Eq. (9). Assuming that the plasma is isothermal within the separatrix, using the constancy of the particle inventory $N = \langle\beta\rangle n_m \pi r_s^2 l$ with $p_m = n_m T_m$, and using radial pressure balance and magnetic flux conservation, we obtain

$$l \propto r_w^{(4-2\gamma)/\gamma}, \quad T_m \propto r_w^{-4(\gamma-1)/\gamma}, \quad n_m \propto r_w^{-4/\gamma}, \quad B_w \propto r_w^{-2}. \tag{16}$$

The scaling laws of Eq. (16) for $\gamma = \frac{5}{3}$ are given in Table I. These scaling laws are independent of the pressure profile, as was also obtained in Sec. II.

For flux compression, r_w is constant but Eq. (15) cannot be readily integrated unless ϵ is a constant as x_s varies. It has been shown[8] that two limiting cases of elongated FRC equilibria are given by sharp-boundary pressure profiles that con-

TABLE I. Adiabatic wall compression scaling laws for $\gamma = \frac{5}{3}$.

l	T_m	n_m	B_w
$r_w^{2/5}$	$r_w^{-8.5}$	$r_w^{-12.5}$	r_w^{-2}

tain the largest and smallest amount of ψ_t. These are the high-flux sharp-boundary and low-flux sharp-boundary models. For these, the values of ϵ are 0 and -1, respectively, and Eq. (15) can be integrated to recover known results[8] for $\gamma = \frac{5}{3}$. For arbitrary diffuse pressure profiles, it can be shown that $\sqrt{2} \leqslant f \leqslant 2/x_s$, where the upper and lower limits correspond to the low-flux and high-flux sharp-boundary models, respectively. From this inequality, we obtain $-1 \leqslant \epsilon \leqslant 0$, which indicates that the scaling laws of flux compression for diffuse profiles are bounded by the two sharp-boundary models. The numerical results of Sec. II show that ϵ is approximately a constant as x_s varies for a given initial $\beta(\phi)$. Even with different initial β profiles, we find that ϵ nearly always lies between -0.2 and -0.3. Therefore, most diffuse profiles scale in flux compression in a way similar to the high-flux sharp-boundary profile for which $\epsilon = 0$. We approximate ϵ by the constant value -0.25 for diffuse profiles and neglect the small variations of less than 10% in the coefficients of Eq. (15) due to departures of ϵ from this value. This approximation is well justified within the one-dimensional model of this work. Then integrating Eq. (15) with the relations $N = \text{const}$, $\psi_t = \text{const}$, $p_m \propto B_w^2$, and $V \propto x_s^2 l$, we obtain

$$
\begin{aligned}
&l \propto x_s^{2(3-\epsilon-\gamma)/\gamma} \langle \beta \rangle^{-(1+\epsilon-\gamma\epsilon)/\gamma}, \\
&T_m \propto x_s^{-2(3-\epsilon)(\gamma-1)/\gamma} \langle \beta \rangle^{(1+\epsilon)(\gamma-1)/\gamma}, \\
&n_m \propto x_s^{-2(3-\epsilon)/\gamma} \langle \beta \rangle^{-(1+\epsilon)(\gamma-1)/\gamma}, \\
&B_w \propto x_s^{-3+\epsilon}.
\end{aligned}
\tag{17}
$$

The scaling laws of Eq. (17) are listed in Table II for the particular case of $\gamma = \frac{5}{3}$ and for three pressure profiles: the high-flux sharp-boundary profile ($\epsilon = 0$), the low-flux sharp-boundary profile ($\epsilon = -1$), and a typical diffuse profile for which we take $\epsilon = -0.25$. In general, an adiabatic compression will involve simultaneous changes of r_w and x_s. The final state can easily be obtained from the initial state by first doing wall compression at constant x_s, using Eq. (16) or Table I, and they by doing flux compression at constant r_w, using Eq. (17) or Table II.

Finally, we compare in Fig. 5 the analytical results of flux compression in this section with the numerical results of Sec. II. We consider the scaling of l as function of x_s. The numerical scaling law obtained with the initial profile $\beta(\phi) = (\phi + \sigma\phi^2)/(1+\sigma)$ is shown in Fig. 5(c). The analytical scaling law obtained from Eq. (17) with $\epsilon = -0.25$ is shown as a dashed line in Fig. 5(d). Within the accuracy of the one-dimensional approximation, the agreement between numerical and analytical results is excellent. We also show in Figs. 5(a) and 5(b) the limiting scaling laws corresponding to the high-flux and low-flux sharp-boundary models. The numerical scaling of l with x_s obtained by Grossmann and Hameiri[5] and given in the Appendix of Ref. 7 suggests larger lengths than those given by Fig. 5(a) for $x_s \leqslant 0.5$. The discrepancy between those results and the ones of Figs. 5(c) and 5(d) may be due to insufficient elongations for small values of x_s in the numerical work of Grossmann and Hameiri to justify the one-dimensional approximation of this work.

TABLE II. Adiabatic flux compression scaling laws for $\gamma = \frac{5}{3}$.

	High-flux sharp boundary	Typical diffuse profile	Low-flux sharp boundary
l	$x_s^{8/5}\langle\beta\rangle^{-3/5}$	$x_s^{19/10}\langle\beta\rangle^{-7/10}$	$x_s^{14/5}\langle\beta\rangle^{-1}$
T_m	$x_s^{-12/5}\langle\beta\rangle^{2/5}$	$x_s^{-13/5}\langle\beta\rangle^{-3/10}$	$x_s^{-16/5}$
n_m	$x_s^{-18/5}\langle\beta\rangle^{-2/5}$	$x_s^{-39/10}\langle\beta\rangle^{-3/10}$	$x_s^{-24/5}$
B_w	x_s^{-3}	$x_s^{-13/4}$	x_s^{-4}

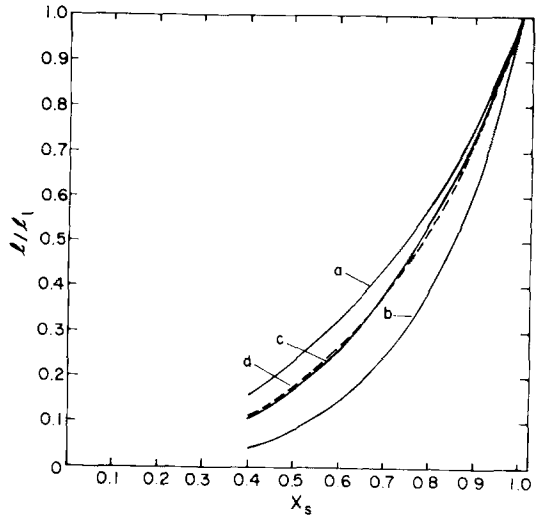

FIG. 5. FRC length as a function of x_s for flux compression. (a) High-flux sharp boundary. (b) Low-flux sharp boundary. (c) One-dimensional compression code. (d) Typical diffuse profile formula from Table II.

IV. CONCLUSION

Two calculations of the adiabatic compression of elongated FRC's have been presented here. The first one uses a long-thin approximation to the MHD entropy function to effect the computation of sequences of adiabatic equilibria with a one-dimensional equilibrium code. The results of this approximate calculation have been checked against a two-dimensional equilibrium code; for ratios of separatrix length to separatrix radius greater than about ten, 10% accuracy is obtained. The second calculation is analytical; it equates the work done on the separatrix with the energy change inside the separatrix. Simple formulas can be obtained by using an approximation. These formulas have the same form as previously published formulas for the high-flux and low-flux sharp-boundary models.[8] The analytic formulas and the one-dimensional compression code were compared. Excellent agreement was obtained for formulas whose exponents were one-fourth of the way from the high-flux exponents to the low-flux exponents as shown in Table II. It is, of course, possible to choose diffuse profiles that violate this rule, but it seems to hold for reasonably smooth ones.

ACKNOWLEDGMENTS

We wish to thank Dr. R. E. Siemon for several valuable discussions.

This work was performed under the auspices of the U. S. Department of Energy.

APPENDIX: MAGNETIC WORK DONE ON THE SEPARATRIX

In this section, we evaluate the work dW done by the external magnetic field on the separatrix. We have

$$dW = F_r dr_s + F_z dl, \tag{A1}$$

where F_r and F_z are radial and axial forces exerted on the separatrix. We consider an elongated FRC equilibrium such as the one of Fig. 1. Neglecting the transition region in the vicinity of $z = l/2$, F_r can be calculated readily as $-2\pi r_s l p_m$ since the magnetic pressure on the elongated cylindrical portion of the separatrix is uniform and equal to $p_m = B_w^2/2\mu_0$.

The axial force F_z can be obtained from considering a control surface $S = \sum_{i=1}^{5} S_i$, as indicated in Fig. 1. In equilibrium, we must have

$$\sum_{i=1}^{5} F_{zi} = 0, \tag{A2}$$

where $F_{zi} = \int\int_{si} (\mathbf{T}\cdot\mathbf{z}) dS_i$ and where $\mathbf{T} = (\mathbf{n}_i\cdot\mathbf{B})\cdot\mathbf{B}/\mu_0 - \mathbf{n}_i \cdot (B^2/2\mu_0)$ is the projection along the surface unit vector $\mathbf{n}_i$ of the Maxwell stress tensor T. Along S_1, $B_1 = B_w$ while flux conservation yields $B_2 = B_w(1 - x_s^2)$ along S_2. Those values are used to obtain $F_{z1} = p_m \pi (r_w^2 - r_s^2)$ and $F_{z2} = -p_m (1 - x_s^2)^2 \pi r_w^2$. We also have $F_{z3} = F_{z5} = 0$ so that Eq. (A2) yields

$$F_z = F_{z4} = -F_{z1} - F_{z2} = -p_m \pi r_s^2 (1 - x_s^2). \tag{A3}$$

Then, Eq. (A1) can be rewritten as

$$dW = -p_m V \left(2\frac{dr_s}{r_s} + (1 - x_s^2)\frac{dl}{l} \right), \tag{A4}$$

where $V = \pi r_s^2 l$ and $dr_s/r_s = dr_w/r_w + dx_s/x_s$. This result can also be obtained by considering the magnetic field energy outside the separatrix. If the separatrix radius and length are changed, holding ψ_0 and r_w fixed, the magnetic energy outside the separatrix will change. The quantity dW is just the negative of this change.

[1] R. E. Siemon, W. T. Armstrong, R. R. Bartsch, R. E. Chrien, J. C. Cochrane, R. W. Kewish, P. L. Klingner, R. K. Linford, J. Lipson, K. F. McKenna, D. J. Rej, E. G. Sherwood, and M. Tuszewski, in *Plasma Physics and Controlled Nuclear Fusion Research* (IAEA, Baltimore, 1982), No. IAEA-CN-41/M-2-1.

[2] A. G. Es'kov, R. H. Kurtmullaev, Ya. N. Laukhin, A. I. Malutin, A. I. Markin, Yu. S. Martushov, O. L. Rostovtsev, V. N. Semenov, and Yu. B. Sosunov, in *Proceedings of the Tenth European Conference on Controlled Fusion and Plasma Physics*, Moscow, 1981 (U. S. S. R. Academy of Sciences, Moscow, 1981), Paper No. L-1.

[3] H. Grad, P. N. Hu, and D. C. Stevens, Proc. Nat. Acad. Sci. USA **72**, 3789 (1975).

[4] R. N. Byrne and W. Grossmann, in *Proceedings of the Third Symposium on Physics and Technology of Compact Toroids in the Magnetic Fusion Energy Program* (LASL, Los Alamos, NM, 1980), p. 138.

[5] W. Grossmann and E. Hameiri, presented at the Sherwood Meeting on Theoretical Aspects of Controlled Thermonuclear Research, Mount Pocono, PA, 1979, Paper No. 2B9.

[6] D. W. Hewett and R. L. Spencer, Phys. Fluids **26**, 1299 (1983).

[7] W. T. Armstrong, R. K. Linford, J. Lipson, D. A. Platts, and E. G. Sherwood, Phys. Fluids **24**, 2068 (1981).

[8] W. T. Armstrong, D. C. Barnes, R. R. Bartsch, R. J. Commisso, C. A. Ekdahl, I. Henins, D. W. Hewett, H. W. Hoida, T. R. Jarboe, C. G. Lilliequist, R. K. Linford, J. Lipson, J. Marshall, K. F. McKenna, J. P. Mondt, D. A. Platts, C. E. Seyler, A. R. Sherwood, E. G. Sherwood, R. E. Siemon, M. Tuszewski, D. V. Anderson, R. Christian, E. H. Klevans, S. Hamasaki, D. D. Schnack, J. M. Sayer, A. I. Shestakov, and J. Killeen, in *Plasma Physics and Controlled Nuclear Fusion Research* (IAEA, Vienna, 1981), Vol. I, p. 481.